Energy transfer enhanced photoluminescence of 2D/3D CsPbBr₃ hybrid assemblies *⊙*

Chenxu Wang ⁽ⁱ⁾; Jinhai Si ⁽ⁱ⁾; Lihe Yan ⁽ⁱ⁾; Ting Li; Xun Hou



J. Chem. Phys. 160, 034704 (2024) https://doi.org/10.1063/5.0187699





Articles You May Be Interested In

Insights into thiocyanate-enhanced photoluminescence in CsPbBr₃ nanocrystals by ultrafast twodimensional infrared spectroscopy

J. Chem. Phys. (May 2024)

The surface chemistry of colloidal lead halide perovskite nanowires

J. Chem. Phys. (April 2024)

 $CsPbBr_3/Cs_4PbBr_6$ NCs glass prepared by a composition regulation strategy for amplification spontaneous emission and white light emitting diode

Appl. Phys. Lett. (October 2021)

Webinar From Noise to Knowledge

May 13th - Register now

Zurich Instruments Konstanz



Energy transfer enhanced photoluminescence of 2D/3D CsPbBr₃ hybrid assemblies

Cite as: J. Chem. Phys. 160, 034704 (2024); doi: 10.1063/5.0187699 Submitted: 15 November 2023 • Accepted: 22 December 2023 • Published Online: 16 January 2024







Chenxu Wang, D Jinhai Si, D Lihe Yan, D Ting Li, and Xun Hou

AFFILIATIONS

Key Laboratory for Physical Electronics and Devices of the Ministry of Education and Shaanxi Key Laboratory of Photonics Technology for Information, School of Electronic Science and Engineering, Xi'an Jiaotong University, No. 28, Xianning West Road, Xi'an 710049, China

^{a)}Author to whom correspondence should be addressed: jinhaisi@mail.xjtu.edu.cn

ABSTRACT

Energy transfer has been proven to be an effective method to optimize optoelectronic conversion efficiency by improving light absorption and mitigating nonradiative losses. We prepared 2D/3D CsPbBr3 hybrid assemblies at different reaction temperatures using the hot injection method and found that the photoluminescence quantum yields (PLQYs) of these hybrids were greatly enhanced from 53.4% to 72.57% compared with 3D nanocrystals (NCs). Femtosecond transient absorption measurements were used to study the PLQY enhancement mechanisms, and it was found that the hot carrier lifetime improved from 0.36 to 1.88 ps for 2D/3D CsPbBr₃ hybrid assemblies owing to the energy transfer from 2D nanoplates to 3D NCs. The energy transfer benefits the excited carrier accumulation and prolonged hot carrier lifetime in 3D NCs in hybrid assemblies, as well as PLQY enhancement in materials.

Published under an exclusive license by AIP Publishing. https://doi.org/10.1063/5.0187699

I. INTRODUCTION

Designing a light-harvesting assembly that mimics natural photosynthesis with a higher efficiency has attracted great interest in the light-energy conversion area. 1-3 In mimicking natural photosynthesis and biological systems, a variety of light absorbers often work together, and regulating energy transfer plays a pivotal role in efficient energy harvesting and optoelectronic applications.^{4,5} Generally, energy transfer can be classified as Dexter type with electron exchange or Förster resonance-based energy transfer (FRET).^{6,7} In some semiconducting devices for solar cells, light-emitting diodes (LEDs), bioimaging, and amplified spontaneous emission using FRET could enable a superior performance by improving light absorption and mitigating nonradiative losses.^{8,9} For instance, Huang et al. demonstrated a 38% increase in power conversion efficiency through FRET-assisted efficient harvesting of photogenerated excitons and long-range exciton migration in polymer-based solar cells upon the inclusion of squaraine. 10 Lin et al. have successfully presented a stepwise FRET strategy for a bright near-infrared system with remarkable persistent luminescence (up to 0.2 s at 810 nm) for bioimaging applications. 11

Since 2014, metal halide perovskite nanocrystals (NCs) have emerged as ideal semiconducting candidates in solar cells, LEDs, lasers, photodetectors, and even photocatalysis because of their excellent absorption coefficient, tunable bandgap, high photoluminescence quantum yields (PLQYs), facile syntheses, and abundant precursor materials. 12-17 In addition, the composition and morphology of perovskite NCs can be precisely controlled upon varying the ligands, reaction temperatures, and precursors, allowing for comprehensive studies on exciton fine structure, level inversion, polaron formation, and especially the energy- and electrontransfer processes. 18-20 For improving the energy transfer efficiency, a directional energy flow based on FRET can be achieved by controlling the perovskite size and morphology. 21-23 This energy funneling results in rapid charge-carrier localization and increased carrier concentration in acceptors, which can enhance the bimolecular recombination rate and facilitate the buildup of population inversion.²⁴

Over the years, efforts have been devoted to the energy transfer between quasi-2D perovskites and 3D bulk perovskites, or perovskite NCs between luminescent molecules. Huang et al. demonstrated an enhanced amplified spontaneous emission in quasi-2D perovskites through a more efficient FRET pathway.²⁵

DuBose and Kamat probed the excited-state interactions with an energy transfer process occurring on the ~200 ps time scale in a CsPbBr₃-Rhodamine B hybrid assembly.²⁶ For 2D nanoplates (NPLs), as the bandgap can be conveniently controlled upon adjusting the layer number, which enables the careful assessment of quantum-confinement effects in the NPLs,27 an energy transfer from 2D NPLs to 3D NCs can be achieved by constructing 2D/3D perovskite hybrids. This could provide an effective way to manipulate the hot carriers in 3D NCs and influence the PL property of perovskite NCs.

In this study, 2D/3D CsPbBr₃ hybrid assemblies were prepared at different reaction temperatures using the hot injection method. Upon changing the reaction temperature from 160 to 80 °C, pure 3D CsPbBr₃ NCs, 2D/3D CsPbBr₃ hybrid assemblies, and 2D CsPbBr3 NPLs were prepared, respectively, which were demonstrated using a transmission electron microscope (TEM) and UV-Vis absorption spectra. We found that the sample prepared at $100\,^{\circ}\text{C}$ had the highest PLQY of 72.57%, and the photoluminescence (PL) enhancement was attributable to more efficient FRET processes. Femtosecond transient absorption measurements were used to examine the FRET process as well as the photoinduced carrier dynamics during the FRET process in the 2D/3D CsPbBr₃ hybrid assemblies.

II. EXPERIMENTAL SECTION

A. Materials

Cesium carbonate (Cs₂CO₃, Aldrich, 99.9% metals basis), lead(II) bromide (PbBr2, Meryer, 99%), oleic acid (OA, Meryer, 85%), oleylamine (OAm, Meryer, C18: 80%-90%), octadecene (ODE, 90%, Aldrich), and hexane (C₆H₁₄, Sinopharm Chemical Reagent Co., Ltd., ≥97.0%) were used. All the chemicals were used without further treatment.

B. Synthesis of Cs-oleate precursor

The cesium oleate solution was prepared following the reported approach by Protesescu et al. 0.412 g of Cs₂CO₃ and 1.25 ml of OA were loaded into a 50 ml three-neck flask along with 20 ml ODE and degassed under vacuum for 10 min followed by purging with N₂ for 10 min at 120 °C by the Schlenk system with continuous magnetic stirring. The process of alternate application of vacuum and N2 was repeated three times to remove the moisture and O2 in the reaction mixture. Then, the temperature of the reaction mixture was increased to 150 °C under N₂ until all Cs₂CO₃ reacted with OA and turned to a yellowish stock of Cs-oleate precursor. Since the Cs-oleate precipitates out of ODE at room temperature, it has to be preheated to 100 °C before injection.

C. Synthesis of 2D/3D CsPbBr₃ hybrid assemblies

10 ml of ODE and 0.138 g of PbBr2 were loaded into a 50 ml three-neck flask and dried under vacuum for 1 h at 120 °C. Dried OAm (1 ml) and dried OA (1 ml) were injected at 120° C under N_2 . After complete solubilization of PbBr₂, the temperature was changed to 80, 100, 120, 140, and 160 °C, and the hot (~100 °C) Cs-oleate solution (0.8 ml in ODE, prepared as described above) was quickly injected, and the reaction mixture was immediately cooled by the ice-water bath. The crude solution was separated by centrifuging

at 10 000 rpm for 5 min, followed by dispersion of precipitation in hexane for further characterization.

D. Characterization

Powder x-ray diffraction was performed using a Shimadzu XRD-6100 diffractometer with Cu-K α radiation ($\lambda = 1.5406$ Å). A UV-2600 spectrophotometer (Shimadzu) was employed to examine the absorption spectra. The photoluminescence spectra were recorded using an OmniFluo-960 spectrometer (Zolix). The timeresolved PL spectra and PLQYs were recorded using a FLS920 spectrometer (Edinburgh). For the time-resolved PL spectra, a picosecond pulsed LED (central wavelength: 375 nm and repetition rate: 10 MHz) was used as the excitation light source. For PLQYs, an excitation light source (400 nm) was selected from the Xe lamp spectrum. Transmitted electron microscopy (TEM) images and high resolution TEM (HRTEM) images were acquired using a JEOL JEM-2100 transmission electron microscope with an acceleration voltage of 200 keV.

E. Femtosecond time-resolved transient absorption

Femtosecond time-resolved transient absorption (TA) measurements were employed on a home-built setup with pump and probe beams generated by a mode locked amplified Ti:sapphire laser system (Coherent Legend, 800 nm, 100 fs, and 1 kHz repetition rate). The 400 nm pump beam was operated at second harmonic generation (SHG) of 800 nm beam. The probe beam, white light continuum (WLC) ranging from 450 to 750 nm, was produced by focusing the 800 nm pulses into a 1-mm-thick sapphire plate. A motorized delay stage was applied to control the delay between the pump and probe pulses. The repetition rate of pump beam was reduced to 500 Hz using a synchronized chopper. The transmitted probe pulses from the samples were collected using a fiber-coupled spectrometer. By comparing the transmitted probe pulses with and without the pump pulse, TA spectra as a function of delay time between the pump and probe pulses were obtained. In the measurements, the samples were filled in 1 mm cuvettes, and the temporal resolution and excitation density are 100 fs and 51 μ J/cm², respectively.

For a typical TA measurement, the TA signal intensity was characterized using optical density expressed by $A_x = \log(I_0/I)$, where I is the transmitted probe light intensity and I_0 is the incident probe light intensity. The time-dependent light-induced absorption change caused by the pump pulse could be evaluated by the difference between probe light intensity measured with (I_{pump}) and without (I_{unpump}) the pump pulse, which was calculated using the following formula:

$$\Delta A(\lambda, t) = \log\left(\frac{I_0}{I_{pump}}\right) - \log\left(\frac{I_0}{I_{umpump}}\right)$$

$$= \log \left(\frac{I_{umpump}}{I_{pump}} \right),$$

where t is the delay time between the pump and probe pulses and λ is the wavelength of the probe light.

III. RESULT AND DISCUSSION

The 2D/3D CsPbBr₃ hybrid assemblies were prepared using the conventional hot injection method at different reaction temperatures, with detailed processes presented in the supplementary material. The samples were prepared with the temperatures set at 160, 140, 120, 100, and 80 °C. As shown using a TEM in Fig. 1(a), 3D CsPbBr₃ NCs without 2D NPLs as control samples with symmetrical nanocubes of 13.3 nm were successfully prepared at 160 °C. Furthermore, the lattice fringes were measured using a high-resolution transmission electron microscope (HRTEM) in Fig. 1(b), which showed lattice spacings of 0.29, 0.41, and 0.59 nm. Combined with x-ray powder diffraction (XRD) characterization [Fig. 1(c)], these lattice spacings corresponded to the (200), (110), and (100) planes of

CsPbBr₃ NCs. The inset in Fig. 1(a) indicates the green emission of a sample excited using 365 nm light.

The TEM and HRTEM micrographs of the products prepared at 140, 120, 100, and 80 °C are shown in Figs. 2(a)–2(h), respectively. As shown in Fig. S1, with decreasing temperature, the size of NCs decreased from 13.3 nm at 160 °C to 9.7 nm at 140 °C and further to 7.2 nm at 120 °C. Moreover, NPLs were formed at a lower reaction temperature, which is similar to the related literature, and their proportion in the products increased as the reaction temperature decreased (as shown in Fig. 2). ^{27–30} It can be seen from the TEM results that most of the NPLs are standing owing to their orient assemblies, making the determination of the formation of nanoplates difficult. Notably, there are also some lying NPLs, which were marked by red dotted frames in

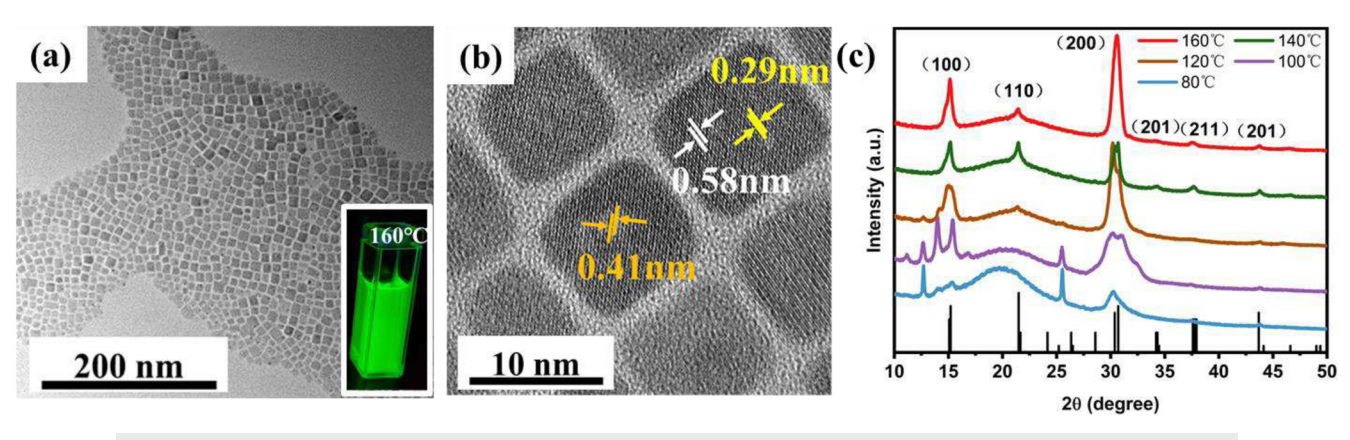


FIG. 1. TEM (a) and HRTEM (b) micrographs for 3D CsPbBr₃ NCs. (c) XRD spectra of samples synthesized at 160, 140, 120, 100, and 80 °C.

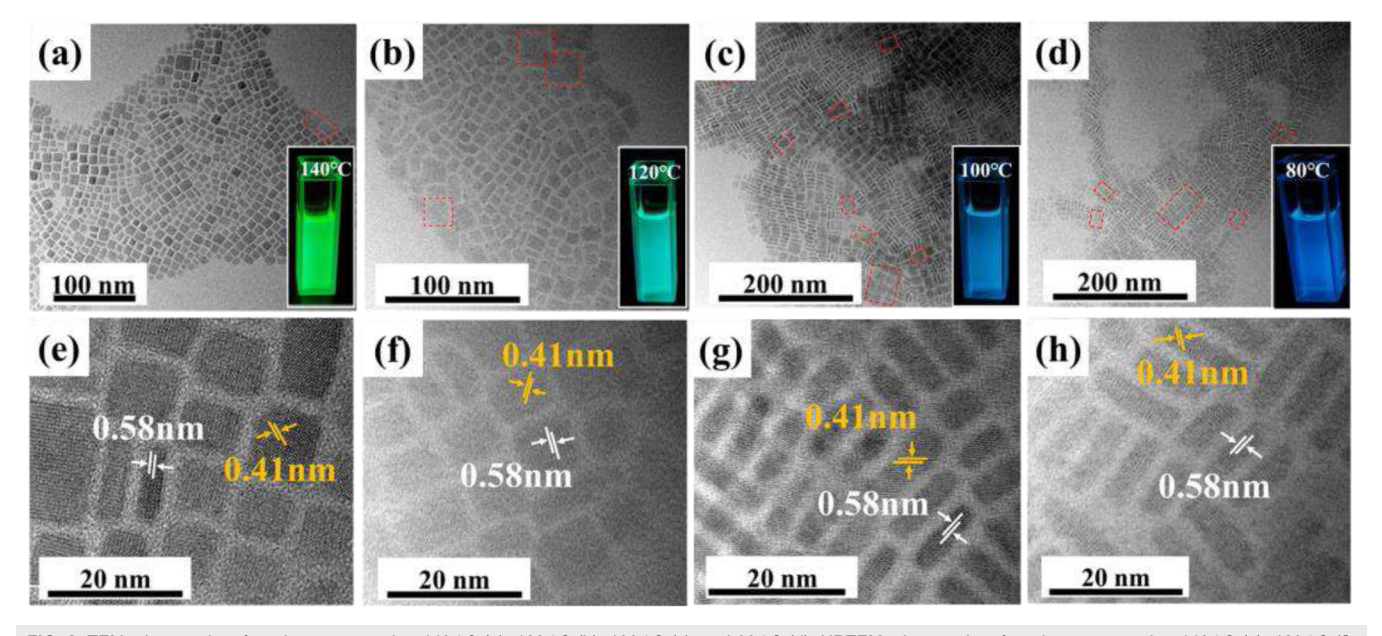


FIG. 2. TEM micrographs of products prepared at 140 °C (a), 120 °C (b), 100 °C (c), and 80 °C (d); HRTEM micrographs of products prepared at 140 °C (e), 120 °C (f), 100 °C (g), and 80 °C (h).

the TEM micrographs and could be the evidence of NPLs. Under 365 nm excitation, the products could emit bright jade green, cyan, turquoise, and blue light at a lower reaction temperature, which was attributable to the formation of smaller NCs and thinner NPLs. The smaller NCs and thinner NPLs enhanced the perovskite quantum confinement and led to PL blueshift. The XRD characterization was used to examine the crystal structure further. Upon comparing with the database, the sample XRD results were in good agreement with the standard XRD patterns, corresponding to the PDF cards of 00-018-0364 for CsPbBr₃ NCs prepared at 140 and 120 °C. To differentiate CsPbBr3 NCs, small-angle diffraction peaks at 120, 100, and 80 °C were used, which were attributable to 2D CsPbBr₃ NPLs. Furthermore, the sample lattice fringes prepared at different temperatures were measured and are shown in Figs. 2(e)-2(h). Consistent with NCs prepared at 160 °C, the lattice spacings of 2D/3D CsPbBr3 hybrid assemblies were 0.41 and 0.59 nm, which corresponded to the (110) and (100) planes of CsPbBr3.

The UV-vis absorption and PL spectra of 2D/3D CsPbBr₃ hybrid assemblies were measured and are shown in Figs. 3(a) and 3(b), respectively. It was clearly observed that the absorption edge of

3D CsPbBr₃ NCs blueshifted from 510 nm (at a preparation temperature of 160 °C) to 499 nm (at a preparation temperature of 100 °C) gradually, which could result from the increasing quantum confinement caused by smaller NCs. Moreover, sharp absorption peaks appeared at preparation temperatures of 120, 100, and 80 °C. These sharp peaks are attributable to exciton absorption within specific layers of 2D NPLs. The absorption peak at 484 nm is attributable to the exciton absorption of five-layer NPLs (n = 5) at a preparation temperature of 120 °C. At a preparation temperature of 100 °C, two absorption peaks at 473 and 484 nm were observed, which corresponded to the exciton absorption of four- and five-layer NPLs (n = 4 and 5). An absorption peak at 410 nm was found at a preparation temperature of 80 °C and was attributable to the exciton absorption of monolayer NPLs (n = 1). However, no monolayer but thicker 2D NPLs were observed in TEM, which might be due to monolayer instability and continuous growth into thicker NPLs. Furthermore, although it was observed using TEM, there was no exciton absorption peak for products prepared at 140 °C, and this was attributable to the low proportion of 2D NPLs. The corresponding products prepared at different temperatures are shown in Table S1.

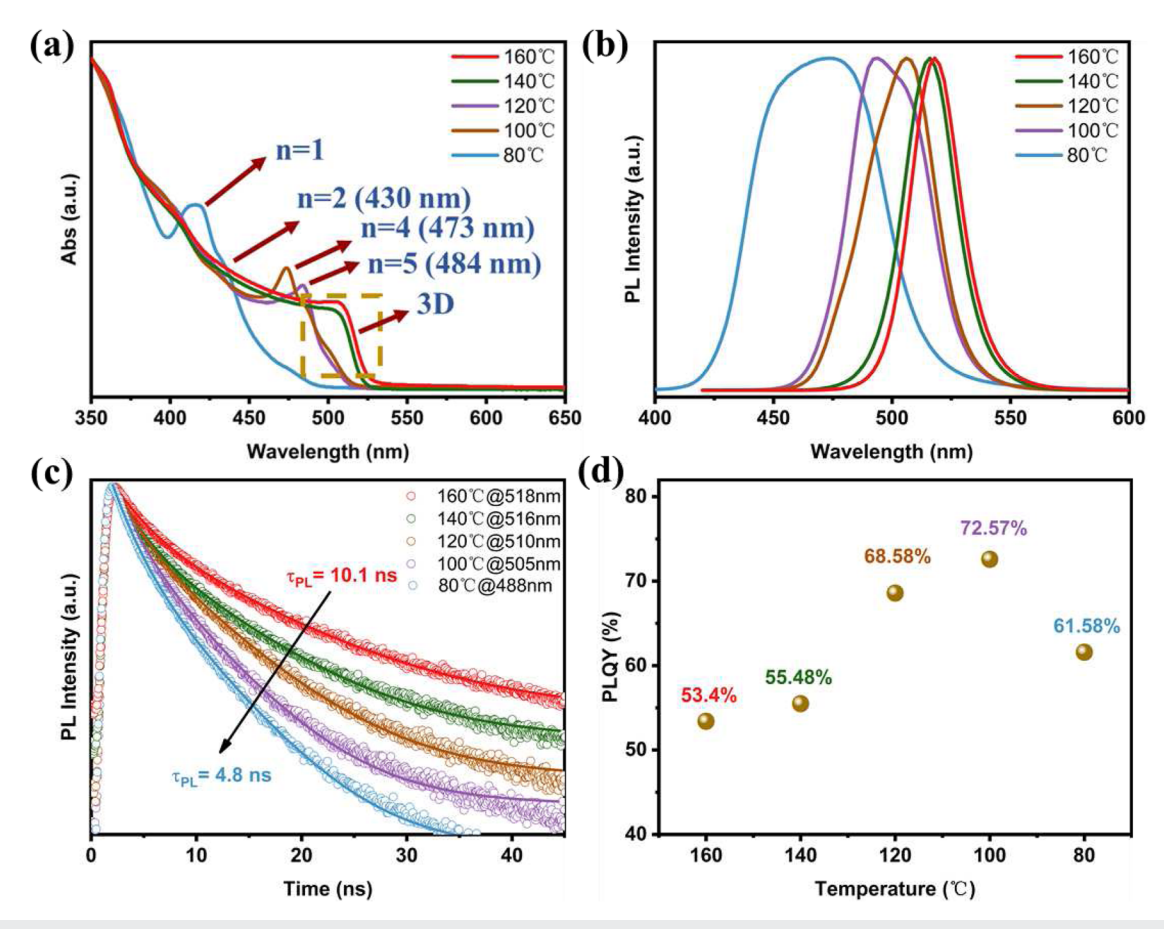


FIG. 3. UV-vis absorption (a) and PL (b) spectra of products at different reaction temperatures; (c) TRPL spectra results of products at different reaction temperatures; and (d) PLQYs of products at different reaction temperatures.

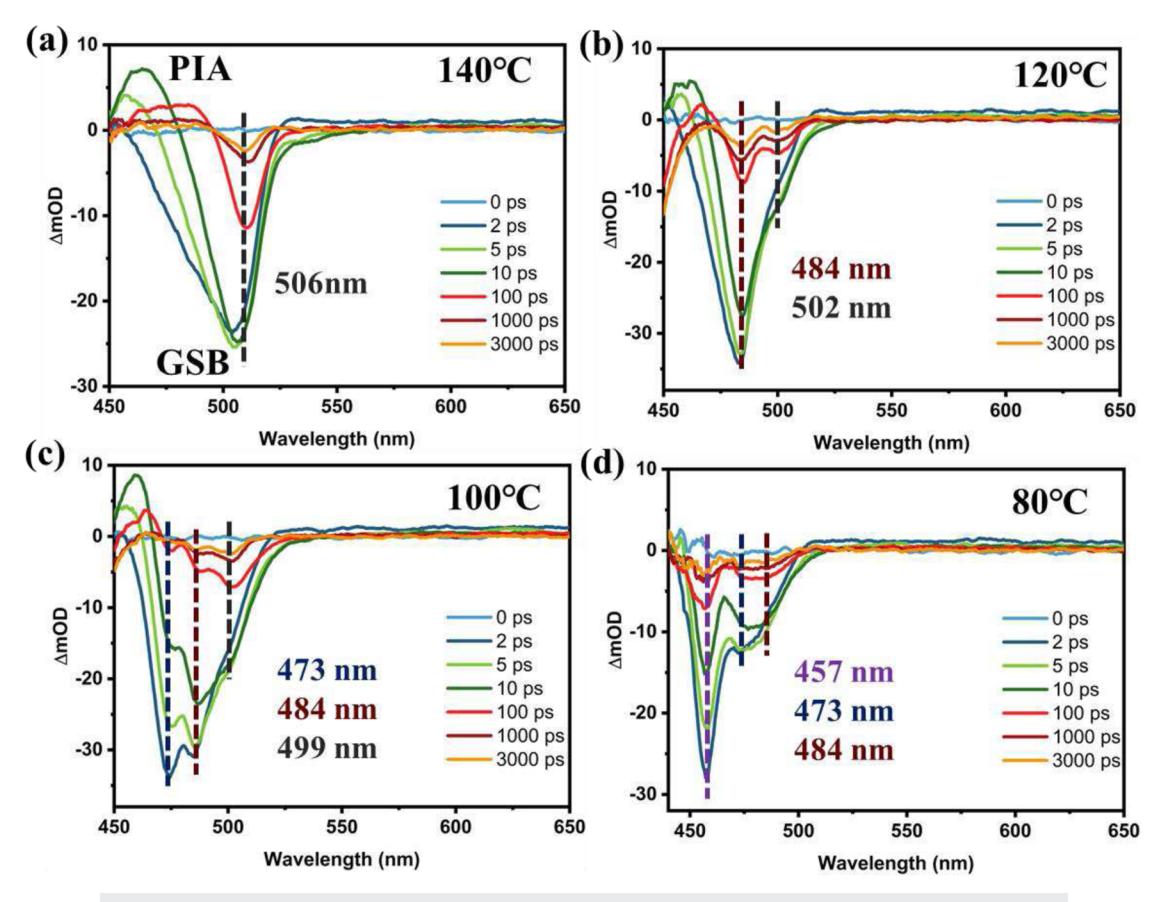


FIG. 4. Transient absorption spectra at selected delay times prepared at 140 °C (a), 120 °C (b), 100 °C (c), and 80 °C (d).

In order to characterize the PL properties, sample PL spectra were obtained at a 400 nm excitation and are shown in Fig. 3(c). As the proportion of 2D NPLs increases, the emission peaks blueshift from 518 nm (at a preparation temperature of 160 °C) to 488 nm (at a preparation temperature of 80 °C). In addition, the PL spectra broadened because of an increase in the 2D NPL content. The time-resolved photoluminescence (TRPL) spectra were characterized to obtain photogenerated carrier dynamics. Based on Fig. 3(c), it was seen that the PL lifetime (the fitted lifetime parameters are shown in Table S2) of the products decreased from 10.1 ns (at a preparation temperature of 160 °C) to 4.8 ns (at a preparation temperature of 80 °C) with an increasing proportion of 2D NPLs. With the size (from 13.3 to 7.2 nm) and dimensionality (from 3D to 2D) reduction of perovskite NCs, the exciton binding energy would be enhanced and result in the expediting of photogenerated carrier recombination rate.^{31–33} Hence, the PL lifetime would be reduced with the preparation temperature decreasing from 160 to 80 $^{\circ}$ C.

To attain the optical conversion performance of the products, an integrating sphere was used to measure the PLQYs [400 nm excitation, filtered from a xenon lamp, Fig. 3(d)]. The PLQY of the sample prepared at 160 °C was 53.4%, which was consistent with the value of 3D CsPbBr₃ NCs in previous reports. ¹² For

pure 2D NPLs prepared at 80 °C, the PLQY was 61.58%, while the PLQYs were significantly increased to 68.58% and 72.57% for the 2D/3D CsPbBr3 hybrid assemblies prepared at 120 and 100 °C, respectively. Charge transfer refers to the electron and/or hole transfer from excited semiconductor nanocrystals to another semiconductor nanocrystals or molecular relay present near the interface.³⁴ Energy transfer often occurs between two materials, of which one is an energy donor and the other is an energy acceptor. The energy transfer occurs due to the charge-charge interaction between oscillating donor and acceptor dipoles in close proximity (1–10 nm).⁷ For the 2D/3D CsPbBr₃ hybrid assemblies prepared in this work, combining with TEM and UV-vis absorption characterization results, the NPLs' emission spectra could overlap with the NCs' absorption, and the distance (1-10 nm) between NPLs and NCs was suitable for energy transfer. Hence, we concluded that the improved PLQYs for 2D/3D CsPbBr₃ hybrid assemblies resulted from an effective energy transfer from NPLs to NCs.

In order to clarify the internal energy transfer mechanism of $2D/3D\ CsPbBr_3$ hybrid assemblies, the synthesized samples were characterized using femtosecond transient absorption (TA) measurements. Femtosecond TA was widely used to investigate the relaxation and transfer processes of photogenerated carriers in

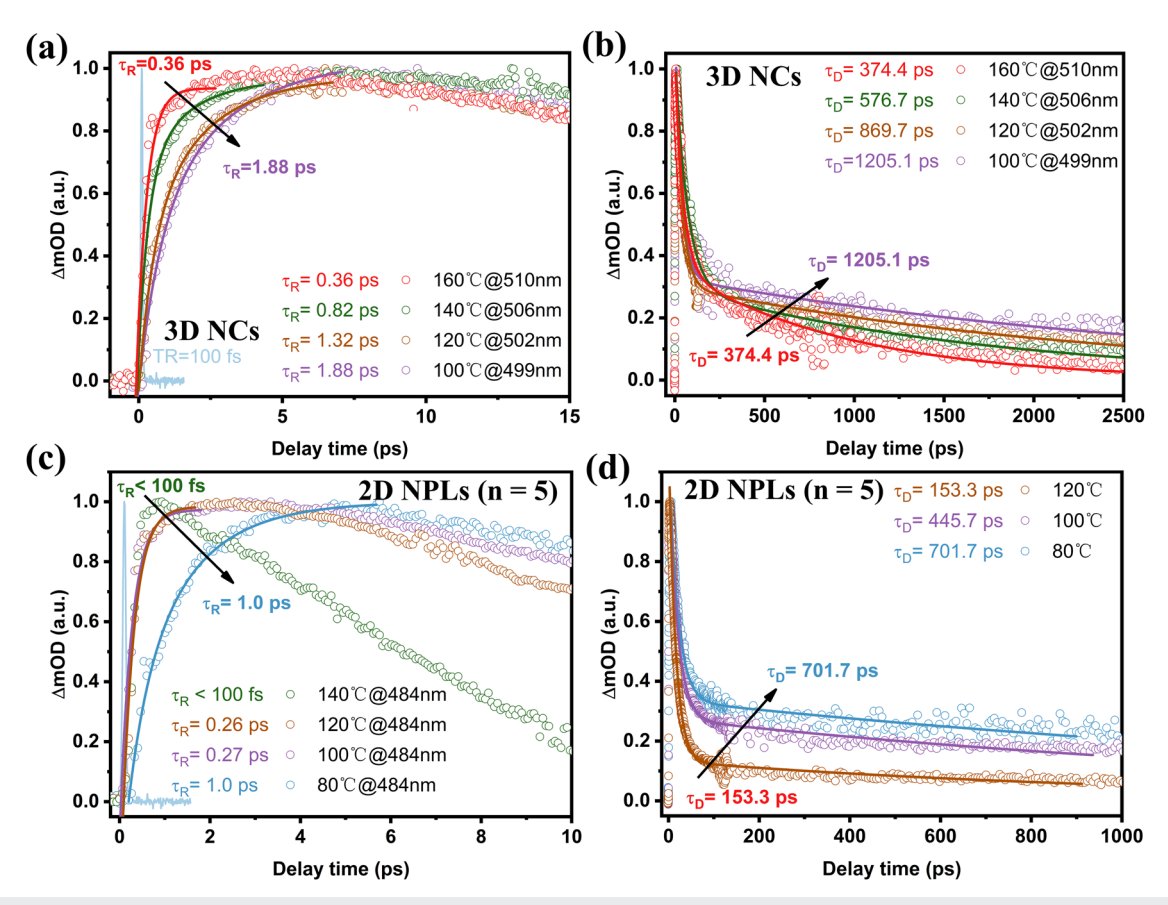


FIG. 5. Rising (a) and relaxation (b) times for the GSB signal of 3D CsPbBr₃ NCs (510, 506, 502, and 499 nm) at different reaction temperatures; the rising (c) and relaxation (d) times for the GSB signal of 2D CsPbBr₃ NPLs at 484 nm (n = 5) at different reaction temperatures. TR: temporal resolution; TR: rising time; and TD: decay relaxation time.

semiconductors.^{35–37} When the CsPbBr₃ NCs were excited, carriers in the valence band (VB) were excited to the conduction band (CB), causing the filling of CB and bleaching of ground state absorption (GSB). The positive peak, namely, photoinduced absorption (PIA), at the blueshift region of the GSB signal, was originated from the absorption arising from the excited state carriers. 38-⁻⁴⁰ Upon comparing the rising and relaxation times of GSB of different samples, the energy transfer process was obtained.³³ The 2D pseudo-color TA spectra for 2D/3D CsPbBr₃ hybrid assemblies are shown in Fig. S2, from which the TA spectra at selected delay times were extracted and are shown in Fig. 4. The negative absorption at 510 and 506 nm was attributable to the GSB effect for 3D CsPbBr₃ NCs prepared at 160 °C (Fig. S3) and 140 °C [Fig. 4(a)], corresponding to the absorption edge of 3D CsPbBr₃ NCs, respectively. With a decrease in preparation temperature, 2D NPLs formed in the products, and the corresponding bleaching signals from the 2D NPL absorption were observed in the TA spectra. The dips at 484 nm in Figs. 4(b)-4(d) corresponded to the bleaching of five-layer NPL absorption, while those at 473 nm in Figs. 4(c) and 4(d) corresponded to the bleaching of four-layer NPL absorption. The dip at 457 nm in Fig. 4(d) corresponded to the bleaching of three-layer NPL absorption. In addition, the GSB signal of 3D CsPbBr₃ NCs absorption blueshifted with decreasing preparation temperature, which resulted from the decreased NC size and increased quantum confinement effect.

The kinetic curves (Fig. 5) for the GSB signal of 3D CsPbBr₃ NCs were extracted to study the development and relaxation dynamics for ultrafast carriers in 2D/3D CsPbBr₃ hybrid assemblies. The rising time for the GSB signal of 3D CsPbBr₃ NCs (499, 502, 506, and 510 nm) and 2D CsPbBr₃ NPLs (n = 5; 484 nm) with different proportions of 2D NPLs was analyzed. From Fig. 5(a), it was observed that the rising time of the GSB signal increased with an increase in 2D NPLs. The rise in the GSB signal for 3D CsPbBr₃ NCs prepared at 160 °C was fitted using a single-exponential function [as shown in Fig. 5(a)], and a fitted rising time of 0.36 ps was attributable to the relaxation of the excited state hot carrier. The rise in the GSB signal for 3D CsPbBr₃ NCs prepared at 140, 120, and 100 °C was fitted using dual-exponential functions, and averaged rising times of 0.82, 1.36, and 1.88 ps were obtained (as shown in Table S3), indicating a longer lifetime for the excited state hot carriers compared with pure 3D NCs. The rise of the GSB signal in 2D/3D CsPbBr₃ hybrid assemblies includes two processes: the fast process (τ₁) in 2D/3D CsPbBr₃ hybrid assemblies could correspond to the hot carrier relaxation time in 3D NCs being

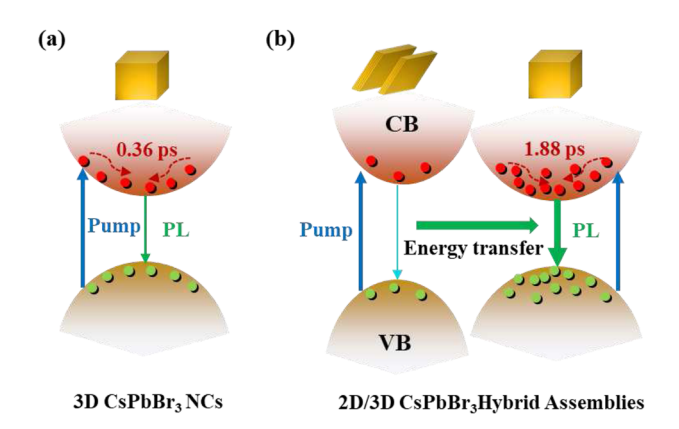


FIG. 6. Schematic of the hot carrier relaxation of 3D CsPbBr₃ NCs and (b) energy transfer of 2D/3D CsPbBr₃ hybrid assemblies. CB: conduction band and VB: valence band.

consistent with the rising time for pure CsPbBr₃ NCs, while the slow process (τ_2) was attributed to the energy transfer from the 2D CsPbBr₃ NPLs to the 3D CsPbBr₃ NCs. Moreover, as shown in Table S3, with the increase ratio of 2D CsPbBr₃ NPLs, the energy transfer time (τ_2) increases from 1.6 ps (140 °C) to 2.9 ps (100 °C), resulting in more carriers accumulated into the 3D CsPbBr₃ NCs with longer hot carrier lifetime for the samples prepared at 100 °C. The energy transfer could not only cause an increase in the rising time of the GSB signal but also prolong the photogenerated carrier lifetime. Figure 5(b) shows the carrier relaxation processes in different samples from the picosecond to the nanosecond region. We found that the effective energy transfer improved the excited state carrier lifetime from 374.7 to 1205.1 ps for 3D CsPbBr₃ NCs prepared at 160–100 °C (the fitted lifetime parameters are shown in Table S4).

In addition to the energy transfer from 2D NPLs to 3D NCs, an energy transfer from thinner (n = 2, 3, and 4) to thicker (n = 5) 2D CsPbBr₃ NPLs also took place. The rising kinetics at 484 nm [n = 5, Fig. 5(c)] were extracted from the TA spectra, and the rising time increased from 0.26 to 1.0 ps (as shown in Table S5) when the reaction temperature changed from 120 to $80\,^{\circ}$ C. The prolonged rising time of the GSB signal for 2D NPLs indicated that an energy transfer from n = 2, 3, and 4 to n = 5 for 2D CsPbBr₃ NPLs occurred in the hybrids. The relaxation dynamics of 484 nm also showed that the energy transfer effectively increased the excited state carrier lifetime, from 153.3 to 701.7 ps, for samples prepared at $120-80\,^{\circ}$ C [as shown in Fig. 5(d), and the fitted lifetime parameters are shown in Table S6].

A model was presented to illustrate these energy transfer processes in the 2D/3D CsPbBr₃ hybrid assemblies, as shown in the diagram of Fig. 6. The hot carrier relaxation process of 3D CsPbBr₃ NCs is shown in Fig. 6(a), which corresponded to a 0.36 ps lifetime. Moreover, as shown in Fig. 6(b), both 2D CsPbBr₃ NPLs and 3D CsPbBr₃ NCs were excited at 400 nm. Due to the overlap of the emission spectrum of 2D CsPbBr₃ NPLs and the absorption spectrum of 3D CsPbBr₃ NCs, an orderly energy transfer could occur in 2D/3D CsPbBr₃ hybrid assemblies, and carriers accumulated gradually, and the hot carrier lifetime improved to 1.86 ps in 3D CsPbBr₃ NCs,

effectively improving the energy utilization efficiency and PLQYs. In our experiments, a higher proportion of 2D CsPbBr₃ NPLs were at lower reaction temperatures, and the energy transfer from 2D CsPbBr₃ NPLs to 3D CsPbBr₃ NCs was more effective, which not only made the carriers collect at the NCs but also increased the hot carrier lifetime. The photogenerated carrier radiation recombination of 3D CsPbBr₃ NCs increased, thus effectively improving the PLQYs.

IV. CONCLUSIONS

In summary, 2D/3D CsPbBr₃ hybrid assemblies were prepared by changing the reaction temperature, and the sample PLQYs improved from 53.4% to 72.57%. The improved PLQY was attributable to energy transfer from 2D NPLs to 3D CsPbBr₃ NCs. The energy transfer mechanism was clarified using femtosecond resolved TA measurements. Upon comparing the rising and decay times for the GSB signal of 3D NCs, an energy transfer from 2D NPLs to 3D NCs was demonstrated. Photogenerated carriers accumulated continuously at the narrow bandgap of 3D CsPbBr₃ NCs, which prolonged the carrier lifetime and further improved the energy utilization efficiency. We believe that this study will provide insights into the energy transfer mechanisms in semiconductor materials.

SUPPLEMENTARY MATERIAL

The supplementary material contains the size distribution of samples prepared at 160, 140, and 120 $^{\circ}$ C (Fig. S1). The 2D pseudocolor TA spectra for all samples (Fig. S2), TA spectra at selected delay time prepared at 160 $^{\circ}$ C (Fig. S3), the table of composition of samples prepared at different temperatures, fitting parameters for PL decays, and TA rising and relaxation processes (Tables S1–S6) are also included in the supplementary material.

ACKNOWLEDGMENTS

This work was supported by the National Research and Development Program of China (Grant No. 2019YFA0706402) and the National Natural Science Foundation of China (Grant No. 62027822).

AUTHOR DECLARATIONS

Conflict of Interest

The authors have no conflicts to disclose.

Author Contributions

Chenxu Wang: Conceptualization (equal); Data curation (lead); Formal analysis (equal); Validation (equal); Visualization (lead); Writing – original draft (equal); Writing – review & editing (equal). Jinhai Si: Conceptualization (equal); Formal analysis (equal); Funding acquisition (equal); Investigation (equal); Project administration (equal); Resources (equal); Supervision (equal); Validation (equal); Visualization (equal); Writing – original draft (equal); Writing –

review & editing (equal). Lihe Yan: Data curation (equal); Funding acquisition (equal); Resources (equal); Visualization (equal); Writing – original draft (equal); Writing – review & editing (equal). Ting Li: Data curation (equal); Investigation (equal); Validation (equal); Writing – review & editing (equal). Xun Hou: Funding acquisition (equal); Methodology (equal); Project administration (equal); Resources (equal); Supervision (equal); Writing – review & editing (equal).

DATA AVAILABILITY

The data that support the findings of this study are available from the corresponding author upon reasonable request.

REFERENCES

- ¹P. V. Kamat, Acc. Chem. Res. **50**(3), 527–531 (2017).
- ²N. S. Lewis and D. G. Nocera, Proc. Natl. Acad. Sci. U. S. A. **103**(43), 15729–15735 (2006).
- ³Y. Wang, H. Suzuki, J. Xie, O. Tomita, D. J. Martin, M. Higashi, D. Kong, R. Abe, and J. Tang, Chem. Rev. **118**(10), 5201–5241 (2018).
- ⁴S. A. Crooker, J. A. Hollingsworth, S. Tretiak, and V. I. Klimov, Phys. Rev. Lett. **89**(18), 186802 (2002).
- ⁵E. Lerner, T. Cordes, A. Ingargiola, Y. Alhadid, S. Chung, X. Michalet, and S. Weiss, Science **359**(6373), eaan1133 (2018).
- ⁶B. Valeur and M. N. Berberan-Santos, *Molecular Fluorescence* (Wiley, 2012).
- ⁷M. Cardoso Dos Santos, W. R. Algar, I. L. Medintz, and N. Hildebrandt, TrAC Trends Anal. Chem. 125, 115819 (2020).
- ⁸ J. I. Basham, G. K. Mor, and C. A. Grimes, ACS Nano 7(6), 1253-1258 (2013).
- ⁹A. A. Mohapatra, V. Kim, B. Puttaraju, A. Sadhanala, X. Jiao, C. R. McNeill, R. H. Friend, and S. Patil, ACS Appl. Energy Mater. 1(9), 4874–4882 (2018).
- ¹⁰ J.-S. Huang, T. Goh, X. Li, M. Y. Sfeir, E. A. Bielinski, S. Tomasulo, M. L. Lee, N. Hazari, and A. D. Taylor, Nat. Photonics 7(6), 479–485 (2013).
- ¹¹F. Lin, H. Wang, Y. Cao, R. Yu, G. Liang, H. Huang, Y. Mu, Z. Yang, and Z. Chi, Adv. Mater. 34, 2108333 (15) (2022).
- ¹²L. Protesescu, S. Yakunin, M. I. Bodnarchuk, F. Krieg, R. Caputo, C. H. Hendon, R. X. Yang, A. Walsh, and M. V. Kovalenko, Nano Lett. 15(6), 3692–3696 (2015).
- ¹³ A. Swarnkar, A. R. Marshall, E. M. Sanehira, B. D. Chernomordik, D. T. Moore, J. A. Christians, T. Chakrabarti, and J. M. Luther, Science 354(6308), 92–95 (2016).
- ¹⁴K. Lin, J. Xing, L. N. Quan, F. P. G. de Arquer, X. Gong, J. Lu, L. Xie, W. Zhao, D. Zhang, C. Yan, W. Li, X. Liu, Y. Lu, J. Kirman, E. H. Sargent, Q. Xiong, and Z. Wei, Nature 562(7726), 245–248 (2018).
- ¹⁵Y. Wang, X. Li, J. Song, L. Xiao, H. Zeng, and H. Sun, Adv. Mater. 27(44), 7101–7108 (2015).
- ¹⁶P. Ramasamy, D.-H. Lim, B. Kim, S.-H. Lee, M.-S. Lee, and J.-S. Lee, Chem. Commun. 52(10), 2067–2070 (2016).

- ¹⁷S. Park, W. J. Chang, C. W. Lee, S. Park, H.-Y. Ahn, and K. T. Nam, Nat. Energy 2(1), 16185 (2016).
- ¹⁸L. Janker, Y. Tong, L. Polavarapu, J. Feldmann, A. S. Urban, and H. J. Krenner, Nano Lett. **19**(12), 8701–8707 (2019).
- ¹⁹M. Gramlich, C. Lampe, J. Drewniok, and A. S. Urban, J. Phys. Chem. Lett. 12(46), 11371–11377 (2021).
- ²⁰ M. G. Greiner, A. Singldinger, N. A. Henke, C. Lampe, U. Leo, M. Gramlich, and A. S. Urban, Nano Lett. 22(16), 6709–6715 (2022).
- ²¹ L. Mishra, R. K. Behera, A. Panigrahi, and M. K. Sarangi, J. Phys. Chem. Lett. 13(19), 4357–4364 (2022).
- ²² L. M. Pazos-Outon, M. Szumilo, R. Lamboll, J. M. Richter, M. Crespo-Quesada, M. Abdi-Jalebi, H. J. Beeson, M. Vrucinic, M. Alsari, H. J. Snaith, B. Ehrler, R. H. Friend, and F. Deschler, Science 351(6280), 1430–1433 (2016).
- ²³C. Cho, B. Zhao, G. D. Tainter, J.-Y. Lee, R. H. Friend, D. Di, F. Deschler, and N. C. Greenham, Nat. Commun. 11(1), 611 (2020).
- ²⁴ L. Lei, D. Seyitliyev, S. Stuard, J. Mendes, Q. Dong, X. Fu, Y. A. Chen, S. He, X. Yi, L. Zhu, C. H. Chang, H. Ade, K. Gundogdu, and F. So, Adv. Mater. **32**, 1906571 (16) (2020).
- ²⁵S. Huang, N. Liu, Z. Liu, Z. Zhan, Z. Hu, Z. Du, Z. Zhang, J. Luo, J. Du, J. Tang, and Y. Leng, ACS Appl. Mater. Interfaces 14(29), 33842–33849 (2022).
- ²⁶ J. T. DuBose and P. V. Kamat, J. Am. Chem. Soc. 143(45), 19214–19223 (2021).
 ²⁷ Y. Bekenstein, B. A. Koscher, S. W. Eaton, P. Yang, and A. P. Alivisatos, J. Am. Chem. Soc. 137(51), 16008–16011 (2015).
- ²⁸Y. Wang, X. Li, S. Sreejith, F. Cao, Z. Wang, M. C. Stuparu, H. Zeng, and H. Sun, Adv. Mater. 28(48), 10637–10643 (2016).
- ²⁹ W. Shen, Y. Yu, W. Zhang, Y. Chen, J. Zhang, L. Yang, J. Feng, G. Cheng, L. Liu, and S. Chen, ACS Appl. Mater. Interfaces 14(4), 5682–5691 (2022).
- ³⁰C. Otero-Martínez, J. Ye, J. Sung, I. Pastoriza-Santos, J. Pérez-Juste, Z. Xia, A. Rao, R. L. Z. Hoye, and L. Polavarapu, Adv. Mater. 34, 2107105 (10) (2022).
- ³¹Y. Li, T. Ding, X. Luo, Y. Tian, X. Lu, and K. Wu, Chem. Mater. **32**(1), 549–556 (2019).
- ³² A. Zhou, Y. Xie, F. Wang, R. Liang, Q. Ou, and S. Zhang, J. Phys. Chem. Lett. 13(20), 4634–4641 (2022).
- ³³B. P. Carwithen, T. R. Hopper, Z. Ge, N. Mondal, T. Wang, R. Mazlumian, X. Zheng, F. Krieg, F. Montanarella, G. Nedelcu, M. Kroll, M. A. Siguan, J. M. Frost, K. Leo, Y. Vaynzof, M. I. Bodnarchuk, M. V. Kovalenko, and A. A. Bakulin, ACS Nano 17(7), 6638–6648 (2023).
- 34 J. T. DuBose and P. V. Kamat, Chem. Rev. 122(15), 12475–12494 (2022).
- ³⁵P. Maity, N. A. Merdad, J. Yin, K. J. Lee, L. Sinatra, O. M. Bakr, and O. F. Mohammed, ACS Energy Lett. **6**(7), 2602–2609 (2021).
- ³⁶S. Panuganti, L. V. Besteiro, E. S. Vasileiadou, J. M. Hoffman, A. O. Govorov, S. K. Gray, M. G. Kanatzidis, and R. D. Schaller, J. Am. Chem. Soc. 143(11), 4244–4252 (2021).
- ³⁷ J. Chakkamalayath, G. V. Hartland, and P. V. Kamat, J. Phys. Chem. C 125(32), 17881–17889 (2021).
- ³⁸T. Huo, L. Yan, J. Si, P. Ma, and X. Hou, J. Mater. Chem. C **11**(11), 3736–3742 (2023)
- ³⁹N. Mondal and A. Samanta, Nanoscale **9**(5), 1878–1885 (2017).
- ⁴⁰C. Wang, L. Yan, J. Si, T. Huo, and X. Hou, J. Alloys Compd. **946**, 169272 (2023).